ELSEVIER

Biosensing under an applied voltage using optical waveguide lightmode spectroscopy

Michelle A. Brusatori, Paul R. Van Tassel *

Department of Chemical Engineering and Materials Science, Wayne State University, 5050 Anthony Wayne Drive, Detroit, MI 48202, USA

Abstract

An applied dc voltage offers a means of controlling immobilization during biosensor fabrication and detection during biosensing application. We present a method to directly and continuously measure the adsorption of biomacromolecules or other polyelectrolytes, under an applied potential difference, based on optical waveguide lightmode spectroscopy (OWLS). An indium tin oxide (ITO) film of thickness ca. 10 nm coated onto a silicon titanium oxide (STO) waveguiding film serves as the working (sensing) electrode. We observe the effective refractive index of the 0th transverse electric guided mode to increase significantly in the presence of an applied potential due to charging of the interfacial double layer and, possibly, modest electrochemical oxidation. Adsorption from solution onto the ITO electrode is detected by a further increase in the effective refractive index. We achieve accurate detection by employing an optical model in which the STO and ITO layers are combined into a single waveguiding film. No improvement is found using models treating the ITO as a separate layer, either dielectric or conducting. Using this method, we find the adsorption of human serum albumin and horse heart cytochrome c to be considerably enhanced in the presence of an applied potential exceeding 1 V. We attribute this behavior to adsorption at positions on the protein molecules of complementary charge.
© 2003 Elsevier Science B.V. All rights reserved.

Keywords: Biosensing; Protein adsorption; Polyelectrolyte adsorption; Dc voltage; Optical waveguide lightmode spectroscopy

1. Introduction

The tailored placement of biomacromolecules or other polyelectrolytes at the liquid–solid interface offers exciting possibilities in biosensing, biocatalysis, tissue engineering, and microelectronics. In many cases, function depends critically on adlayer structure. As (1) adlayer formation typically occurs by adsorption from solution; and (2) the adsorbing species typically possesses a permanent charge distribution, a promising means of structural control is the application of a direct current (dc) potential during the formation process. In order to optimally incorporate an applied voltage into an overall design strategy, one must understand its influence on the adsorption process and, ultimately, adlayer structure. Methods for analyzing the formation

process in the presence of an applied potential are therefore needed. In this paper, we introduce a means to measure the adsorption of biomacromolecular species under closed circuit conditions using optical waveguide lightmode spectroscopy (OWLS).

Several methods have been proposed for measuring biomacromolecular adsorption in the presence of an applied voltage (or, equivalently, a given surface charge density). Of these, perhaps the simplest (albeit ex situ) method is to apply a standard immunoassay following exposure of a two-electrode system to a protein solution (Burns et al., 1996). A more promising method involves the determination of the capacitance of the electrical double layer that forms spontaneously at the interfacial region of a charged surface and an electrolytic solution (Feng and Andrade, 1994; DeFicquelmontLoizos et al., 1997; Fievet et al., 1998; Omanovic and Roscoe, 1999, 2000; Oliva et al., 2001; Phillips et al., 2001). This measurement is made via the ac impedance in the presence of a dc bias and yields information on the surface coverage and structure of the adsorbed layer. A

---

* Corresponding author. Present address: Department of Chemical Engineering, Yale University, New Haven, CT 06520, USA. Tel.: +1-203-432-7983; fax: +1-203-432-7983.

E-mail address: paul.vantassel@yale.edu (P.R. Van Tassel).

disadvantage is the requirement of certain unproven assumptions relating protein density and structure to the double layer capacitance. Total internal reflection fluorescence allows for the direct measurement of adsorbed mass under an applied voltage, but requires the attachment of fluorescent labels (Fraaije et al., 1990; Asanov et al., 1997, 1998; Liron et al., 2002). Quartz crystal vibrational analysis is possible (Khan and Wernet, 1997), but a careful accounting of the viscous drag of the contacting liquid is necessary for signal quantification. Optical reflectometry is another promising method for measuring biomacromolecular adsorption under an applied potential difference (Bos et al., 1994; Kleijn et al., 1996; Barten et al., in preparation).

Of particular value would be a technique capable of providing precise and continuous kinetic measurements of biomacromolecular adsorption under an applied potential. Kinetic data are useful in elucidating and quantifying the mechanisms of the adsorption process and may act as a biosensing signal. OWLS (Tiefenthaler and Lukosz, 1989; Lukosz et al., 1991; Nellen and Lukosz, 1993; Ramsden, 1993; Lukosz, 1995; Ramsden, 1999; Voros et al., 2002) is a highly sensitive optical method capable of continuous macromolecular adsorption measurements with a time resolution of ca. 3 s and a density resolution of ca. 1 ng/cm^2. Detection is based on the influence of an adsorbed layer on the planar waveguide modes excited by a polarized monochromatic light impinging on an embossed diffraction grating. Previous applications employed waveguiding films of poorly conducting materials such as silicon titanium oxide (STO), thus preventing the use of this method to investigate adsorption in the presence of a potential difference. Very recently, however, a waveguiding film coated with a conducting layer of indium tin oxide (ITO) has been introduced (Stankowski and Ramsden, 2002). In this work, we (i) present a biosensing method based on OWLS with ITO-coated waveguiding films (Brusatori, 2001); (ii) demonstrate accurate detection under an applied potential using an optical model treating the STO and ITO films as a single optical layer; and (iii) report the first OWLS measurements of macromolecular adsorption under an applied voltage.[1]

2. Materials and methods

2.1. Sensor chip

An ITO coated OW 2400 sensor chip (MicroVacuum Ltd., Budapest) is employed (see Figs. 1 and 2 and Table
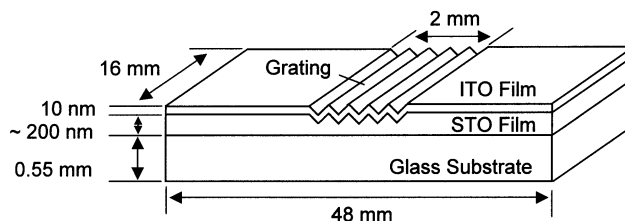
---

[1] We note that Bearinger et al. (in preparation) have concurrently developed an OWLS method for detecting biomacromolecular adsorption under an applied voltage.

Fig. 1. A schematic of the ITO coated OW 2400 sensor chip (Micro Vacuum Ltd., Budapest). Physical and chemical propertied of the STO and ITO layers are given in Table 1.
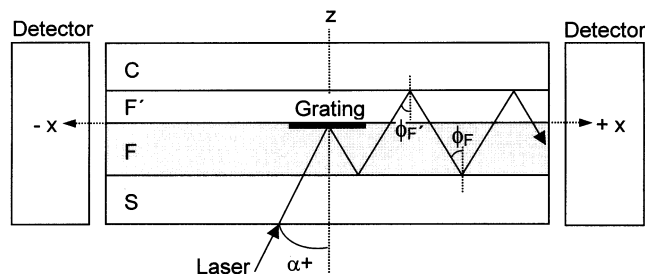

Fig. 2. A schematic of the sensor chip as a four-layer optical waveguide. Monochromatic light penetrates a glass substrate (S) at an angle α and is coupled into a waveguiding film (F) via a grating. A second film (F′), representing either a conducting layer or adsorbed species, may separate the waveguiding layer from the cover (C) solution. A guided mode is detected when the phase shift of one complete period of total internal reflection equals an integral multiple of 2π. The guided mode is characterized by propagation angles ϕ_F and $\phi_{F'}$.

1). The adsorbing surface is a 10 nm film of ITO resting on a ca. 200 nm STO waveguiding film, itself supported on a glass substrate. A diffraction grating of depth 20 nm and length 2 mm is embossed into the top surface of the STO film to allow for optical coupling. The In/Sn ratio of the ITO film is 2.0 ± 0.1, as measured by XPS, and its water contact angle is $48.1 \pm 1.3°$, as measured using a contact angle goniometer (model NRL 100, RameHart). The contact angle did not change under an applied potential difference of 5.0 V between the ITO and a Pt wire submerged in the contacting drop.

2.2. Optical waveguide lightmode spectroscopy (OWLS)

All OWLS experiments reported here are performed using a BIOS-1 instrument (MicroVacuum, Budapest) consisting of a sensor chip and a modified flow cell (see below), mounted to the head of a precision goniometer, and a He–Ne laser whose polarized beam is of wavelength $\lambda = 632.816$ nm and of diameter 0.8 mm. The sensor chip, shown in Figs. 1 and 2, consists of an optical waveguide (F) resting on a glass support (S). A second film (F′) may separate the waveguiding layer from the cover (C) solution. As described further in Section 3.1, the F and F′ layers may represent distinct STO and ITO films, or a composite STO–ITO wave-

Table 1
Chemical and physical properties of the ITO-coated OW 2400 sensor chip, as shown in Fig. 1

	ITO film	STO film	Glass substrate
Material	$In_{2-2x}Sn_xO_{3-x}$ ($x = 0.50 \pm 0.02$)	$Si_{1-x}Ti_xO_2$ ($x = 0.25 \pm 0.05$)	SiO_2
Refractive index	$1.78 - 0.03$ i	1.77 ± 0.03	1.52578
Thickness	10 nm	170–220 nm	0.55 mm
Linear resistance	208 Ω/cm		

guiding film and an adsorbed layer. During an experiment, the sensor chip is rotated relative to the laser beam and the intensity of light exiting the two ends of the film is measured by photodetectors. This intensity is a maximum when a stable, transverse field and coherent propagation in the x (horizontal) direction occurs. Propagation is characterized by angles ϕ_F and $\phi_{F'}$, as shown in Fig. 2. An analysis of the governing optics and their use in OWLS to detect macromolecular adsorption is given in Section 3.1.

2.3. Flow cell

A flow cell (Fig. 3) is constructed to enable liquid to contact the sensor chip at the grating region and to allow for a voltage difference across the adsorbing surface at a controlled temperature (Brusatori, 2001). A disk shaped platinum electrode is mounted flush with the upper face of the flow cavity parallel to and 1.0 mm above the surface of the sensor chip; it serves as the counter electrode. The ITO coated sensor chip acts as the working electrode. Electrical contact is made through the end of a small steel rod, located outside the flow chamber, pressed against the ITO film.

The flow cell is sealed to the surface of the sensor chip with a (n-buna) gasket to create a flow cavity of volume 70 mm^3. Fluid is drawn into the cavity via a peristaltic pump through a 0.762 mm ID bore in the solid interior of the flow cell and exits through an outlet bore of the same dimension. The total length of the inlet line is 21.0 cm (5.8 cm inlet bore plus a 15.2 cm Teflon tubing). The flow cavity is a rectangular channel of dimensions 12.7 mm × 5.5 mm × 1.0 mm. Assuming fully developed Poiseuille flow in the flow cavity, the shear rate is $a = 6F/wh^2$, where F is the volumetric flow rate and w and h are as described in Fig. 3.

The cell is maintained at a constant temperature by thermostatic circulating water inside the Teflon flow cell body. The large thermal mass of the flow cell mediates any ambient temperature fluctuations. Teflon is chosen for its chemical resistance to most solvents as well as its thermal and electrical insulating properties.
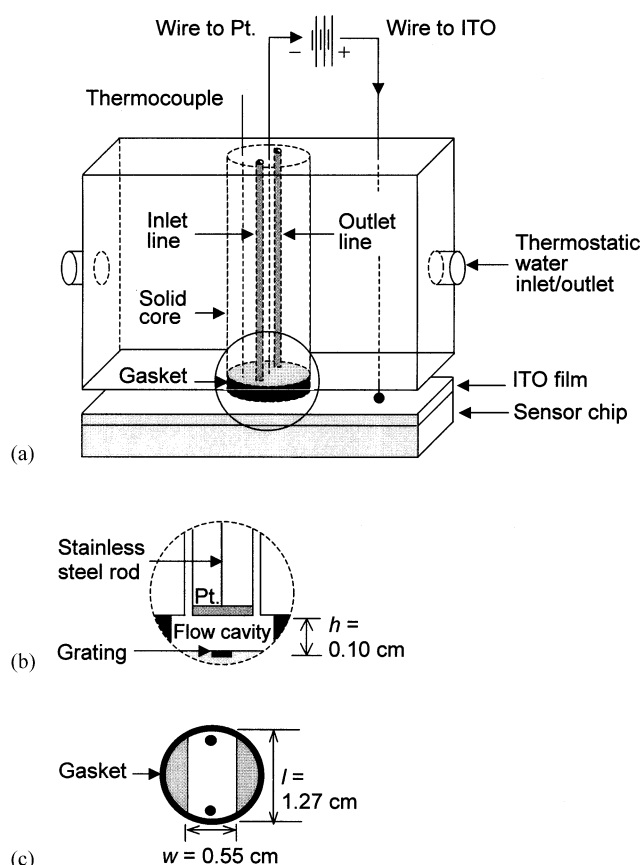

Fig. 3. (a) A schematic of the flow cell sealed to an ITO coated sensor chip. The inlet and outlet lines are in thermal contact with a teflon thermostatic circulating chamber to control the temperature in the flow cavity (monitored by a thermocouple). (b) A close-up of the flow cavity whose upper and lower bases are the ITO and Pt electrodes, repectively, and whose walls are an n-buna gasket. (c) A top view of the flow cavity.

2.4. Proteins

Human serum albumin (fraction V[1]) has a molecular weight of 66,300 and an isoelectric point of 4.7. Cytochrome c (type IV) has a molecular weight of 12,370 and an isoelectric point of 10, and its iron–porphyrin complex exhibits a redox potential of + 0.251 V (vs. standard hydrogen electrode) (Dryhurst et al., 1982). Both proteins are purchased from the Sigma Chemical Company. Aqueous solutions of 0.1 mg/ml are prepared by dissolving the protein in deionized water (of

pH 5.5–6.0 and conductivity 1.30 ± 0.05 μS at 25 °C) for 30 min at 37 °C. Solutions not used within 8 h are discarded. Deionized water is chosen as the protein solvent rather than buffer solutions of higher ionic strength in order to minimize double layer screening and thus enhance voltage effects. The conductivities of prepared aqueous albumin and cytochrome c solutions are determined experimentally to be 3.8 ± 0.3 and 7.2 ± 0.4 μS, respectively, at 25 °C.

2.5. Equivalent electric circuit

In an equivalent electrical circuit representation of the biosensing system (Fig. 4), the ITO film of the sensor chip and the solution inside of the flow cavity contribute as resistors and the two solution-electrode interfaces each act as a resistor and a capacitor in parallel. Current flow through the system is measured via the voltage drop across an external 100 kΩ resistor. The applied voltage, $\Delta V = V_{ITO} - V_{Pt}$, across the ITO and platinum electrodes is measured with a voltmeter connected beyond the external resistor. The resistances of the wires, connectors, and platinum are negligible.

An electrometer (model 6514, Keithley Co., Ohio) is used to measure the ITO electrode potential relative to that of a Au reference electrode in deionized water. The reference electrode registers a potential of 0.689 ± 0.001 V vs. a standard hydrogen electrode (SHE) and is placed in a solution reservoir. All electrode potentials are reported with respect to the SHE. An analysis of the biosensing system's current response to an applied voltage is given in Section 3.2.

2.6. Experimental procedure

Prior to use, an ITO coated sensor chip is soaked for ca. 24 h in deionized water (without protein) in order to avoid a signal drift due to gradual filling of the porous waveguiding film with solvent (Ramsden, 1994). The sensor chip is inserted into the flow cell assembly, which is then mounted to the rotating head of the biosensing system. Deionized water is drawn into the flow cavity via a peristaltic pump at a rate of 1.33 mm³/s, corresponding to a wall shear rate of about 1.5/s. The temperature of the external water bath is adjusted to maintain the body of the flow cell at 25 ± 0.5 °C. A tracking experiment is performed where the effective refractive indices associated with the transverse electric and transverse magnetic modes are recorded every 23.5 s. Once a stable baseline is achieved, a dc voltage is applied across the ITO and platinum electrodes ($\Delta V = V_{ITO} - V_{Pt}$). For a positive applied voltage, the ITO (Pt) electrode acts as the anode (cathode).

The application of a dc potential difference causes N_{TE} and N_{TM} to increase sharply, then quickly plateau ($0 < \Delta V < 1.5$ V) (see Fig. 5) or gradually decrease reaching steady values within an hour ($\Delta V > 1.5$ V). The application of a negative voltage causes the ITO to become opaque, probably due to an electrochemical reduction, and thus become useless as an OWLS sensing substrate (Stankowski and Ramsden, 2002). After recording stable values of N_{TE} and N_{TM} for 15–20 min, a protein solution is drawn into the flow cavity of the sensor chip/flow cell assembly at a rate of 1.33 mm³/s and adsorption is monitored for ca. 1 h. Following completion of an experiment, the electrodes are disconnected from the power supply and all surfaces (contacting the protein), including the sensor chip, are cleaned with a 1% solution of Terg-A-Zyme (a laboratory detergent with protease from Alconox) in deionized
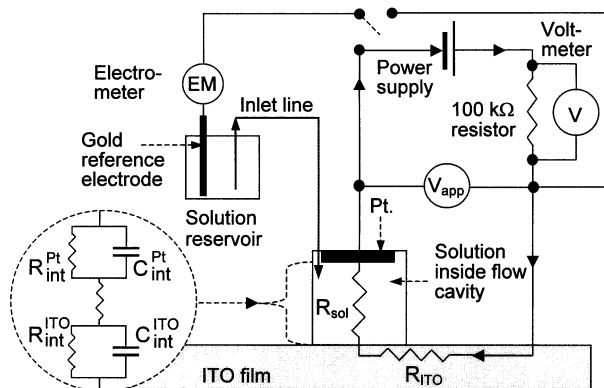

Fig. 4. An electrical circuit schematic of the biosensing system. Both ITO- and Pt-solution interfaces are treated as a resistor and a capacitor in parallel. The solution and the ITO film also act as resistors. The current is measured across a 100 kΩ external resistor. An electrometer is used to measure the potential of the ITO or Pt electrodes relative to that of a Au reference electrode in deionized water, whose potential relative to a SHE is 0.689 ± 0.001 V.
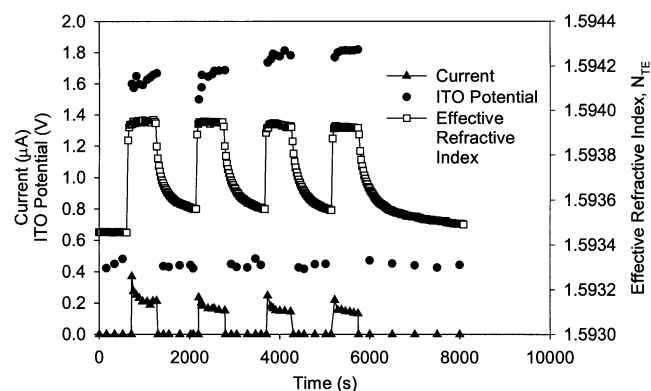

Fig. 5. The electric current, the ITO electrode potential (vs. SHE), and the effective refractive index versus time for deionized water as measured by the biosensing system alternating between an open circuit potential ($\Delta V_{OCP} = -0.02 \pm 0.01$ V) and an applied dc voltage of $\Delta V = 1.0$ V. The charging of the interfacial double layers, and perhaps a modest oxidation of the ITO layer, cause the observed changes.

water. The sensor chip is cleaned in an ultrasonic bath, of frequency 5.5×10^4 Hz, containing the cleaning solution for 600 s and then rinsed extensively with deionized water. The flow cell and tubing as washed by allowing the cleaning solution to flow through at a rate of 1.33 mm^3/s for 1200 s, followed by a 1200 s rinse with deionized water. This cleaning procedure has been implemented in previous work and has shown a high degree of reproducibility (Calonder et al., 2001; Calonder and Van Tassel, 2001).

Conversion of the OWLS output signal, as described in Section 3.1, requires certain known parameters. The refractive index of the solution, n_C, is measured using a refractometer (AR600, Leica Micrsystems, Buffalo) at a wavelength of 632.8 nm. The refractive index of glass, n_S, as provided by the sensor chip manufacturer, is 1.52578 at 25 °C. The refractive index and thickness of the waveguiding film(s) (n_F, d_F, $n_{F'}$, and $d_{F'}$) are determined independently with the OWLS instrument from baseline data generated prior to the onset of adsorption. The refractive index change with concentration, $\partial n_C / \partial c$, is taken to be 0.188 cm^3/g (de Feijter et al., 1978).

3. Theory

3.1. Optical waveguide analysis

We consider a four-layer optical waveguide composed of a glass support (S), a waveguiding film (F), a second film (F'), and a cover solution (C) (see Fig. 2). As described further below, the F' layer may represent an adsorbed layer or the second layer of a two-layer waveguiding film. A polarized laser beam penetrates the glass support of the sensor chip and according to

$$N \equiv n_F \sin \phi_F = n_{air} \sin \alpha + l\lambda/\Lambda, \tag{1}$$

where N is the effective refractive index, n_F is the film's refractive index, ϕ_F is the propagation angle, n_{air} is the refractive index of air, α is the incident angle of the laser beam, λ is its wavelength, l is the diffraction order of the grating, and Λ is the grating period. The condition under which a coherent propagation occurs through the waveguide in the x (horizontal) direction is

$$2k_{z,F}d_F + \varphi_{F,S} + \varphi_{F,F',C} = 2\pi n, \tag{2}$$

where $k_{z,F}$ is the z (vertical) component of the wave vector, d_F is the thickness of the waveguiding film, $k_{z,F}d_F$ is the phase shift due to the wave traversing the film, $\varphi_{F,S}$ and $\varphi_{F,F',C}$ are the phase shifts associated with total internal reflection at the F,S and F,F',S interfaces, respectively, and the integer m is the mode number (only the $m = 0$ mode is supported by our sensor chips).

The phase shift at a given interface is related to its (complex) reflection coefficient by $r = |r|e^{i\varphi}$. For a simple interface between films α and β,

$$r_{\alpha,\beta} \equiv \frac{k_{z,\alpha}/n_\alpha^{2\rho} - k_{z,\beta}/n_\beta^{2\rho}}{k_{z,\alpha}/n_\alpha^{2\rho} + k_{z,\beta}/n_\beta^{2\rho}}, \tag{3}$$

where $\alpha, \beta = $ S, F, F', or C, n_α is the refractive index of film α, and the vertical component of the wave vector is defined as

$$k_{z,\alpha} = \frac{2\pi}{\lambda} n_\alpha \cos(\phi_\alpha), \tag{4}$$

where ϕ_α is the propagation angle in film α. (A simple application of Snell's law shows $\cos(\phi_\alpha) = \sqrt{1 - N^2/\text{Re}(n_\alpha)^2}$, where $\text{Re}(n_\alpha)$ is the real part of the refractive index.) In Eq. (3), $\rho = 0$ or 1 for electric field vectors oriented perpendicular (transverse electric or TE mode) or parallel (transverse magnetic or TM mode) to the plane of incidence, respectively. The reflection coefficient across the F,F',C interface is given by (Tiefenthaler and Lukosz 1989)

$$r_{F,F',C} = \frac{r_{F,F'} + r_{F',C}e^{i\delta}}{1 + r_{F,F'}r_{F',C}e^{i\delta}}, \tag{5}$$

where

$$\delta = 2k_{z,F'}d_{F'} + \frac{4\pi i}{\lambda} \text{Im}(n_{F'})d_{F'} \tan(\phi_{F'}) \sin(\phi_{F'}), \tag{6}$$

and $\text{Im}(n_{F'})$ is the imaginary part of the refractive index. The phase shifts $\varphi_{F,S}$ and $\varphi_{F,F',C}$ are expressed in terms of the associated reflection coefficient by $\varphi = \arcsin[\text{Im}(r)|r|]$, where $|r|$ is the magnitude of r.

In the above analysis, the F and F' layers may represent distinct STO and ITO films, or a composite STO–ITO film and an adsorbed layer (the validity of treating the STO and ITO films as a single layer is tested in Section 4). In the former case, $n_{F'}$ is complex due to it being a conducting layer. In all cases, n_C, $n_S < N < \text{Re}(n_{F'})$, so the laser light penetrates the F,F' interface and undergoes total internal reflection at the F,S and F',C interfaces. The vertical wave vector components $k_{z,C}$ and $k_{z,S}$ are thus purely imaginary, indicating evanescent waves.

When the F' layer consists of an adsorbed species, Eq. (2) may be solved for both TE and TM modes, yielding $n_{F'}$ and $d_{F'}$. The density of the adsorbed layer may be approximated by (de Feijter et al., 1978)

$$\Gamma = \frac{(n_{F'} - n_C)d_{F'}}{\partial n_C/\partial c}, \tag{7}$$

where $\partial n_C/\partial c$ is the change in the refractive index with concentration (c).

3.2. Electrical circuit analysis

We consider an equivalent electrical circuit in which the ITO layer and the solution within the flow cell act as resistors and the two interfaces each act as a resistor and a capacitor in parallel (Fig. 4). The current through this circuit is related to the total applied voltage by

$$\Delta V = IR + I_{int}^{ITO} R_{int}^{ITO} + I_{int}^{Pt} R_{int}^{Pt}, \tag{8}$$

where I is the total current, $I_{int}^{ITO}(I_{int}^{Pt})$ and $R_{int}^{ITO}(R_{int}^{Pt})$ are the currents and resistances at the ITO (Pt) interfaces, respectively, and R is the resistance due to the ITO and solution: $R = R_{ITO} + R_{sol}$. The interfacial currents are related to the associated capacitances via

$$I_{int}^{ITO} R_{int}^{ITO} = \frac{1}{C_{int}^{ITO}} \int_0^t (I - I_{int}^{ITO}) dt' \tag{9a}$$

$$I_{int}^{Pt} R_{int}^{Pt} = \frac{1}{C_{int}^{Pt}} \int_0^t (I - I_{int}^{Pt}) dt'. \tag{9b}$$

Combining Eqs. (8) and (9), one obtains the following coupled ordinary differential equations:

$$\frac{dX}{dt} = AX + B, \quad X(0) = 0 \tag{10}$$

where X and B are the following 2×1 matrices:

$$X = \begin{bmatrix} I_{int}^{ITO} \\ I_{int}^{Pt} \end{bmatrix} \tag{11a}$$

$$B = \begin{bmatrix} \dfrac{\Delta V}{C_{int}^{ITO} R_{int}^{ITO} R} \\ \dfrac{\Delta V}{C_{int}^{Pt} R_{int}^{Pt} R} \end{bmatrix} \tag{11b}$$

and A is the following 2×2 matrix:

$$A = \begin{bmatrix} -\dfrac{1}{C_{int}^{ITO} R} - \dfrac{1}{C_{int}^{ITO} R_{int}^{ITO}} & -\dfrac{R_{int}^{Pt}}{C_{int}^{ITO} R_{int}^{ITO} R} \\ -\dfrac{R_{int}^{ITO}}{C_{int}^{Pt} R_{int}^{Pt} R} & -\dfrac{1}{C_{int}^{Pt} R} - \dfrac{1}{C_{int}^{Pt} R_{int}^{Pt}} \end{bmatrix} \tag{12}$$

The solution to Eq. (10) is

$$X = (e^{At} - U)A^{-1}B \tag{13}$$

where U is the 2×2 identity matrix. This solution is more conveniently expressed in terms of the eigenvalues and eigenvectors of A as follows:

$$X = E \Lambda E^{-1} A^{-1} B \tag{14}$$

where E is the matrix of eigenvectors to A and Λ is the following 2×2 matrix:

$$\Lambda = \begin{bmatrix} e^{\lambda_1 t} - 1 & 0 \\ 0 & e^{\lambda_2 t} - 1 \end{bmatrix} \tag{15}$$

In Eq. (15), λ_1 and λ_1 are the two (negative) eigenvalues of A.

The total current I, obtained by inserting the interfacial currents of the 2×1 matrix X into Eq. (8), is thus expected to decay via a double exponential toward a steady-state value.

4. Results

We begin by reporting changes in effective refractive index (N_{TE}), electrode potential, and current brought about by the application of a dc potential bias in the presence of deionized water. In Fig. 5, we show these quantities as functions of time for an alternate application of an open circuit potential ($\Delta V_{OCP} = -0.02 \pm 0.01$ V) and a potential difference of $\Delta V = V_{ITO} - V_{Pt} = 1.0$ V. We observe both the current and the ITO potential to increase abruptly upon application of voltage and the former (latter) to gradually decrease (increase) thereafter. Upon removal of the applied potential, these quantities quickly revert to their original values. These observations are consistent with a gradual charging of the ITO/solution and Pt/solution interfacial double layer capacitors predicted quantitatively in Section 3.2. The corresponding initial (asymptotic) overall resistance of the equivalent electrical circuit of Fig. 4 is 32 MΩ (67 MΩ). We observe N_{TE} to rapidly increase upon voltage application but to decay quite slowly following a return to open circuit potential; these changes likely reflect the presence of charged species in and around the sensor chip and/or the mild electrochemical oxidation of ITO. A voltage-induced orientation of water in the porous ITO film is also a possible explanation, as suggested elsewhere (Stankowski and Ramsden, 2002). We also observe good reproducibility over several voltage applications. (The slight drifts in current and ITO potential may reflect irreversible electrochemical oxidation of ITO.)
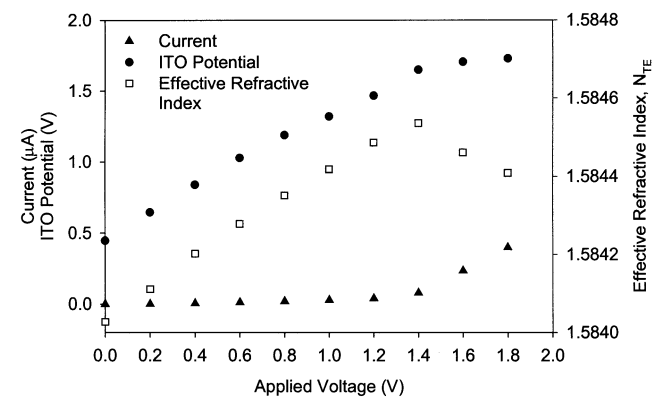

Fig. 6. The asymptotic current, ITO electrode potential (vs. SHE), and effective refractive index versus applied dc voltage for the biosensing system containing deionized water. The increase in current beyond an applied potential of 1.5 V signals the onset of hydrolysis.

In Fig. 6, we show the asymptotic current, ITO potential, and 0th TE mode effective refractive index versus applied voltage. The increased current above 1.5 V signifies the onset of appreciable hydrolysis; this appears to cause a decrease in N_{TE} as well. (Hydrogen and oxygen appear to remain solvated, however, as we observe no gas formation.) Applying a potential of the opposite sign, where the ITO film acts as the cathode, we find the optical properties of the film to change dramatically due a reduction of the ITO, making the sensor chip unusable for OWLS experiments.

It is clearly desirable to convert effective refractive index to adsorbed density, but doing so brings forth two important questions: (1) Must the ITO layer be considered explicitly, and if so, must the imaginary portion of its complex refractive index be considered? (2) Do the model equations of Section 3.1 hold under an applied voltage? To answer these questions, we measure the refractive index of a (non-adsorbing) 5.0 mg/ml glucose solution in water, with and without an applied dc potential, using three different waveguide models: (i) a three-layer model in which the STO and ITO films are considered to be a single layer (i.e. both reflection coefficients are determined via Eq. (3)); (ii) a four-layer model in which $n_{F'}$ is real (i.e. the F′ layer is a dielectric); and (iii) a four-layer model in which $n_{F'}$ is complex (i.e. the F′ layer is a conductor). The refractive index of the glucose solution is $1.33173 \pm 1 \times 10^{-5}$ as measured by an Abbey refractometer. In Table 2, we show refractive index values obtained using the biosensing system within each of the three waveguide models for cases of open circuit potential and an applied voltage of $\Delta V = 5$ V. We observe all values to be within 3×10^{-5} of one another. Since the difference $(n_F - n_C)$ appearing in Eq. (7) is

typically around 0.5, uncertainty of this magnitude has no appreciable effect on a measured adsorbed density. Thus, we conclude that an applied voltage has only a negligible effect on the instrument's detection and that one may consider the STO and ITO films as a single effective film. (A related analysis on films consisting of distinct adsorbed multilayers arrived at the same conclusion (Picart et al., 2001).)

In Figs. 7 and 8, we show the measured adsorbed densities of albumin and cytochrome c as functions of time, under different applied potentials, on two different sensor chips. We observe the adsorption rate and the steady state adsorbed density to significantly increase with increasing applied potential. In fact, beyond a threshold voltage, the adsorption curves fail to reach a plateau. Interestingly, this trend is similar for both proteins despite the difference in overall net charge (albumin is negative and cytochrome c is positive at the experimental pH). We attribute this behavior to strong interactions between the surface and locally charged regions of the protein. In the case of cytochrome c, the fraction of adsorbed molecules with iron porphyrin groups of oxidation states 2 and 3 differs according to the electrode potential. However, since even the open circuit potential of ITO greatly exceeds the standard redox potential of $+0.251$ V (Fig. 6), we expect adsorption onto ITO under all positive applied voltages to occur principally in the oxidized state.

Although these trends hold for different sensor chips, we do observe variability of up to 20%, probably due to microstructural surface differences between chips. We find a much smaller variability (ca. 8%) for multiple runs on the same sensor chip (separated by cleaning procedures as described in Section 2.5).

In Figs. 9 and 10, we show current and adsorbed protein density as a function of time for albumin and

Table 2
The refractive index, n_C, of a 5.0 mg/ml glucose solution—for an open circuit potential and an applied voltage of 5 V—as determined using (i) a three-layer waveguide model where the STO and ITO layers are treated as a single layer; (ii) a four-layer waveguide model where the ITO film is treated as a separate dielectric layer (i.e. of real refractive index); and (iii) a four-layer waveguide model where the ITO film is treated as a separate conducting layer (i.e. of complex refractive index)

Open circuit potential	Three-layer waveguide model with composite STO–ITO layer	$n_C = 1.33177 \pm 1 \times 10^{-5}$
Open circuit potential	Four-layer waveguide model with dielectric ITO layer	$n_C = 1.33178 \pm 1 \times 10^{-5}$
Open circuit potential	Four-layer waveguide model with conducting ITO layer	$n_C = 1.33177 \pm 1 \times 10^{-5}$
$\Delta V = 5$ V	Three-layer waveguide model with composite STO–ITO layer	$n_C = 1.33175 \pm 2 \times 10^{-5}$
$\Delta V = 5$ V	Four-layer waveguide model with dielectric ITO layer	$n_C = 1.33175 \pm 2 \times 10^{-5}$
$\Delta V = 5$ V	Four-layer waveguide model with conducting ITO layer	$n_C = 1.33175 \pm 2 \times 10^{-5}$

The closeness of the values demonstrates the validity of treating the STO and ITO films as a single optical layer and the accuracy of detection in the presence of an applied voltage.
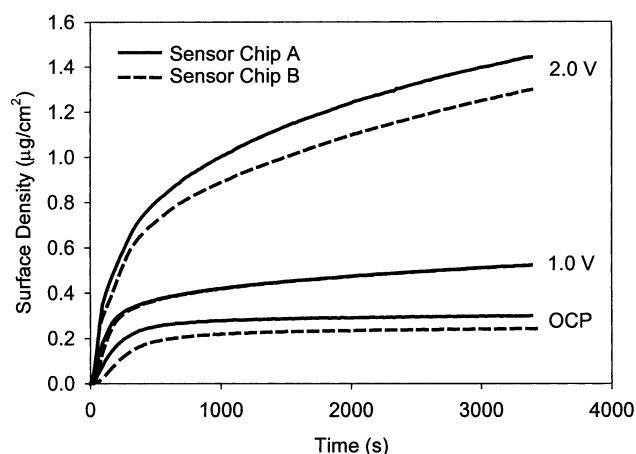

Fig. 7. The density of adsorbed albumin versus time from a 0.1 mg/ml solution for an open circuit potential and applied dc potentials 1.0 and 2.0 V on two different sensor chips. The increased adsorption at higher applied voltages is attributed to an affinity between negatively charged regions of the protein and the ITO surface.
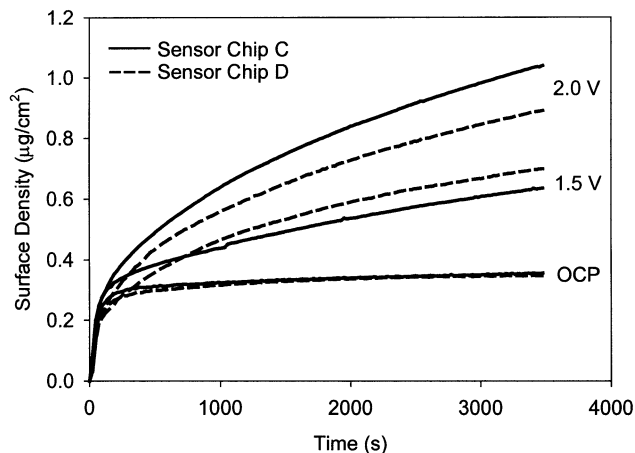
Fig. 8. The density of adsorbed cytochrome c versus time from a 0.1 mg/ml solution for an open circuit potential and applied dc potentials 1.5 and 2.0 V on two different sensor chips. The increased adsorption at higher applied voltages is attributed to an affinity between negatively charged regions of the protein and the ITO surface.
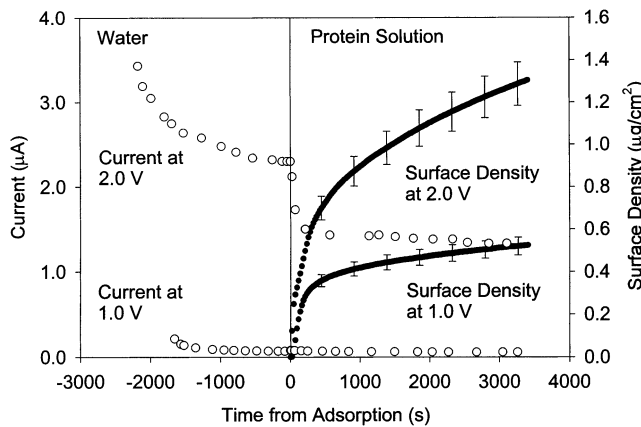

Fig. 9. The density of adsorbed albumin and the associated current versus time from a 0.1 mg/ml solution for applied dc potentials of 1.0 and 2.0 V. The current decrease during initial adsorption is due to an influence on the ITO and Pt interfacial double layers and a blocking of electrochemically active sites by adsorbed proteins.

cytochrome c. We observe the current to decrease initially (or, for the lower voltage, to remain essentially unchanged) upon addition of an albumin solution and to increase initially upon addition of a cytochrome c solution. Three factors are at play here. At both the ITO and Pt electrodes, adsorption of either protein is both affecting the interfacial charge distribution and covering surface sites at which electrochemical reactions take place (e.g. involving dissolved hydrogen). Adsorption of cytochrome c may additionally be accompanied by an oxidation or reduction of the iron porphyrin group, depending on electrode potential.[2] The first two of these

Fig. 10. The density of adsorbed cytochrome c and the associated current versus time from a 0.1 mg/ml solution for applied dc potentials of 1.0 and 2.0 V. The current increase during initial adsorption is due to an electrochemical reaction of the iron porphyrin group with the ITO and Pt electrodes.

effects tend to reduce current and together explain the behavior observed for albumin. The third effect tends to increase current and explains the behavior observed for cytochrome c.

5. Conclusions

An important accomplishment here is the modification of an OWLS biosensor for the continuous measurement of biomacromolecular adsorption under a dc potential applied between an ITO-coated waveguiding sensor chip and a Pt counter-electrode. We show the effective refractive index of the 0th TE guided mode to increase significantly in the presence of an applied potential due to charging of the interfacial double layer and, possibly, modest electrochemical oxidation. Nonetheless, an optical model in which the STO and ITO layers are treated as a single waveguiding film yields an accurate measure of the refractive index of a contacting solution and the density of an adsorbed protein layer. We also show an applied potential to significantly increase the extent of protein adsorption, irrespective of the overall protein charge, and attribute this to adsorption at complementarily charged patches. The ability to deposit a high-density protein layer, without a high bulk concentration or a long adsorption time, may be significant in biosensing and other applications.

---

[2] We note that for $\Delta V < 1.5$ V, cytochrome c is oxidized at both the ITO and Pt electrodes (albeit to a lesser extent at the Pt surface). Cytochrome c is reduced at the Pt electrode for $\Delta V > 1.5$ V.
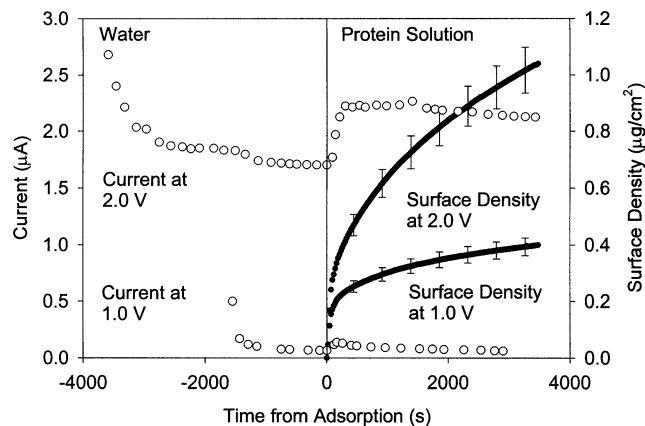
References

Asanov, A.N., DeLucas, L.J., Oldham, P.B., Wilson, W.W., 1997. Heteroenergetics of bovine serum albumin adsorption from good solvents related to crystallization conditions. J. Colloid Interface Sci. 191, 222–235.

Asanov, A.N., Wilson, W.W., Odham, P.B., 1998. Regenerable biosensor platform: a total internal reflection fluorescence cell with electrochemical control. Anal. Chem. 70, 1156–1163.

Barten, D., Kleijn, M., Cohen Stuart, M.A. In preparation.

Bearinger, J.P., Voros, J., Textor, M., Spencer, N.D., Hubbell, J.A. EC OWLS, A novel technique for engineering and characterizing surfaces. Pilot study with PLL-PEG. In preparation.

Bos, M.A., Shervani, Z., Anusiem, A.C.I., Giesbers, M., Norde, W., Kleijn, J.M., 1994. Influence of the electric potential of the interface on the adsorption of proteins. Colloids Surfaces B: Biointerfaces 3, 91–100.

Brusatori, M.A. (2001). Ph.D. Thesis, Protein adsorption kinetics under an applied electric field: an optical waveguide lighmode spectroscopy study, Wayne State University.

Burns, N.L., Holmberg, K., Brink, C., 1996. Influence of surface charge on protein adsorption at an amphoteric surface: effects of varying acid to base ratio. J. Colloid Interface Sci. 178, 116–122.

Calonder, C., Tie, Y., Van Tassel, P.R., 2001. History dependence of protein adsorption kinetics. Proc. Natl. Acad. Sci. USA 98, 10 664–10 669.

Calonder, C., Van Tassel, P.R., 2001. Kinetic regimes of protein adsorption. Langmuir 17, 4392–4395.

de Feijter, J.A., Bejamins, J., Veer, F.A., 1978. Biopolymers 17, 1759.

DeFicquelmontLoizos, M.M., Takenouti, H., Kante, W., 1997. Long-time and short-time investigation of the electrode interface through electrochemical impedance measurements. Application to adsorption of human serum albumin onto glassy carbon rotating disc electrode. J. Electroanal. Chem. 428, 129–140.

Dryhurst, G., Kadish, K.M., Scheller, F.W., Renneberg, R., 1982. Biological Electrochemistry. Academic Press, New York.

Feng, L., Andrade, J.D., 1994. Protein adsorption on low-temperature isotropic carbon. 2. Effects of surface-charge of solids. J. Colloid Interface Sci. 166, 419–426.

Fievet, P., Mullet, M., Reggiani, J.C., Pagetti, J., 1998. Influence of surface charge on adsorption of a hydrophobic peptide onto a carbon surface by capacitance measurement's. Colloid Surf. A-Physicochem. Eng. Asp. 144, 35–42.

Fraaije, J., Kleijn, J.M., Vandergraaf, M., Dijt, J.C., 1990. Orientation of adsorbed cytochrome-c as a function of the electrical potential of the interface studied by total internal-reflection fluorescence. Biophys. J. 57, 965–975.

Khan, G.F., Wernet, W., 1997. Adsorption of proteins on electroconductive polymer films. Thin Solid Films 300, 265–271.

Kleijn, M., Stuart, M.C., deWit, A., 1996. Electro-optic effect in the solid phase of the indium tin oxide electrolyte solution interface observed by reflectometry. Colloid Surf. A-Physicochem. Eng. Asp. 110, 213–217.

Liron, Z., Tender, L.M., Golden, J.P., Ligler, F.S., 2002. Voltage-induced inhibition of antigen–antibody binding at conducting optical waveguides. Biosens. Bioelectron. 17, 489–494.

Lukosz, W., 1995. Integrated optical chemical and direct biochemical sensors. Sens. Actuator B-Chem. 29, 37–50.

Lukosz, W., Clerc, D., Nellen, P.M., Stamm, C., Weiss, P., 1991. Output grating couplers on planar optical wave-guides as direct immunosensors. Biosens. Bioelectron. 6, 227–232.

Nellen, P.M., Lukosz, W., 1993. Integrated optical input grating couplers as direct affinity sensors. Biosens. Bioelectron. 8, 129–147.

Oliva, F.Y., Avalle, L.B., Macagno, V.A., De Pauli, C.P., 2001. Study of human serum albumin–TiO2 nanocrystalline electrodes interaction by impedance electrochemical spectroscopy. Biophys. Chem. 91, 141–155.

Omanovic, S., Roscoe, S.G., 1999. Electrochemical studies of the adsorption behavior of bovine serum albumin on stainless steel. Langmuir 15, 8315–8321.

Omanovic, S., Roscoe, S.G., 2000. Interfacial behavior of beta-lactoglobulin at a stainless steel surface: an electrochemical impedance spectroscopy study. J. Colloid Interface Sci. 227, 452–460.

Phillips, R.K.R., Omanovic, S., Roscoe, S.G., 2001. Electrochemical studies of the effect of temperature on the adsorption of yeast alcohol dehydrogenase at Pt. Langmuir 17, 2471–2477.

Picart, C., Ladam, G., Senger, B., Voegel, J.C., Schaaf, P., Cuisinier, F.J.G., Gergely, C., 2001. Determination of structural parameters characterizing thin films by optical methods: a comparison between scanning angle reflectometry and optical waveguide lightmode spectroscopy. J. Chem. Phys. 115, 1086–1094.

Ramsden, J.J., 1993. Review of new experimental-techniques for investigating random sequential adsorption. J. Stat. Phys. 73, 853–877.

Ramsden, J.J., 1994. Porosity of pyrolyzed sol–gel wave-guides. J. Mater. Chem. 4, 1263–1265.

Ramsden, J.J., 1999. OWLS: a versatile technique for sensing with bioarrays. Chimia 53, 67–71.

Stankowski, S., Ramsden, J.J., 2002. Voltage-dependent coupling of light into ITO-covered waveguides. J. Phys. D-Appl. Phys. 35, 299–302.

Tiefenthaler, K., Lukosz, W., 1989. Sensitivity of grating couplers as integrated-optical chemical sensors. J. Opt. Soc. Am. B-Opt. Phys. 6, 209–220.

Voros, J., Ramsden, J.J., Csucs, G., Szendro, I., De Paul, S.M., Textor, M., Spencer, N.D., 2002. Optical grating coupler biosensors. Biomaterials 23, 3699–3710.